Proceedings of the
International Conference on Mechanical Engineering 2009
(ICME2009) 26- 28 December 2009, Dhaka, Bangladesh

ICME09-FM-13

COMBINED EFFECTS OF CURVATURE AND TORSION ON FLUID FLOW IN A HELICAL RECTANGULAR DUCT

P. Kumar Bhattacharjee[1] and M. Mahmud Alam[2]

[1]Natural Science Group, National University, Gazipur, Bangladesh
[2]Mathematics Discipline, Khulna University, Khulna, Bangladesh

ABSTRACT

This paper is concerned with the steady incompressible fully developed flow through a left-handed helical rectangular duct and presents the flow structure for various Dean number (D_n), non-dimensional torsion (τ') and non-dimensional curvature (κ') at aspect ratio $\gamma = 1.5$. Numerical study is performed to investigate the flow characteristics under various flow conditions. The flow structure in the helical rectangular duct is investigated numerically to examine the combined effects of non-dimensional curvature and torsion. Spectral method is used as a main tool for numerical calculations, where the Chebyshev polynomial, the collocation methods, the Arc-length method and the Newton-Raphson method are also used as secondary tools.

Keywords: Curvature, Torsion, Rectangular Duct.

1. INTRODUCTION

The flows through curved and helical ducts are encountered in various industrial processes. Flows in separation processes, heat exchangers, physiological systems, chemical processes, medical equipments and centrifugal compressors are examples of such processes. At first, Dean[1] formulated the curved pipe problem in mathematical terms under the fully developed flow conditions. He found the two-vortex counter rotating secondary flow patterns originated by the centrifugal force. Since then, there have been a lot of theoretical and experimental work concerning this flow and the review articles by Berger et al.[2] and Ito[3] may be referred. Cheng et al.[4] reported two-vortex secondary flow patterns in a curved duct with square cross-section by using finite difference method. One of the interesting phenomena of flow through the curved duct is the bifurcation of the flow. Yang and Wang[5] studied numerically the bifurcation structure and stability of the solutions of fully developed viscous flow in curved square duct. The governing equations were discretized by using the finite volume method.

The helical duct has been used extensively in various industrial applications to enhance the rate of heat, mass and momentum transfers. In order to improve the performance of these devices, an accurate and reliable analysis of the flow in the helical duct is necessary, which can also be used as the basis for studying the flow in other devices. The geometry of a helical pipe, as shown in Fig 1, is characterized by the curvature and torsion. These non-dimensional curvature and torsion are defined respectively as, $\kappa' = \frac{r'}{r'^2 + \alpha'^2}$, $\tau' = \frac{\alpha'}{r'^2 + \alpha'^2}$ where r' is the radius of the helix and $\alpha' = \frac{pitch}{2\pi}$. The secondary flow caused by the centrifugal force due to curvature can be affected by torsion. If the pitch is equals to zero, then the torsion is equals to zero and the helical duct reduces to a toroidally curved duct. In a helical duct the centrifugal force plays an important role in creating a pair of vortices. However, above a critical value of the Dean number $\left(D_n = \frac{\sqrt{2\kappa'}a^3}{\mu\upsilon} G \right)$, the secondary flow is changed from the appearance of several pair of vortices structure, due to the balance of the acting centrifugal and pressure gradient forces on the flow. The torsion causes the distortion in the symmetry of the flow, enlarging the upper vortex of the secondary flow at the expense of the lower vortex. Wang[6] was the pioneer author who formulated the helical pipe flow for circular cross-section using non-orthogonal co-ordinates and analyzed the flow for small curvature and torsion by taking series expansions of these parameters. He found that the secondary flow is a single vortex cell. There have been very few studies regarding the torsion effect on the flow in a helical square duct or rectangular duct. The effect of small torsion on the helical square ducts has been

[1] *O.S.D., Directorate of Secondary and Higher Education Dhaka,, Bangladesh.*

investigated by Bolinder and sunden[7] and Sakalis et al.[8]. Recently, Bhattacharjee and Alam[9] investigated the torsion effect on fluid flow in a helical square duct. They found the bifurcation flow structure. They also found that multiple pair of vortices appeared on the bifurcation areas. Again, Wang and Andrews[10] investigated the flow in a helical rectangular duct. They studied the effect of the pitch ratio, pressure gradient and curvature ratio on the velocity distribution and fluid resistance in fully developed laminar flow of an incompressible fluid in a helical rectangular duct.

The main object of the present study is to investigate numerically the flow through a *left-handed helical rectangular duct* for a wide range of the Dean number, torsion and curvature. The non-dimensional governing equations have been solved numerically by employing spectral method as a main tool.

2. Governing Equations

A viscous incompressible fully developed steady flow through a *left-handed* helical duct with rectangular cross-section as shown in Figure 1 is considered. Let $2a$ and $2b$ be the width and the height of the cross–section respectively.

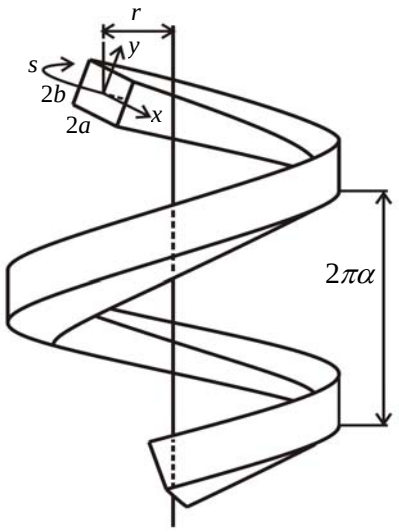

Fig 1. Helical duct with rectangular cross-section.

Thus, the Continuity and Navier-Stokes equations in terms of curvilinear co-ordinates are given by

$$\frac{\partial}{\partial \xi^i}\left(\sqrt{g}\; q_j\; \gamma_j^i\right) \;=\; 0 \qquad (1)$$

$$\gamma_j^k\left(\frac{\partial q_i}{\partial \xi^k} - q_l E_{lik}\right) q_j \;= -\frac{1}{\rho}\frac{\partial p}{\partial \xi^j}\gamma_i^j$$
$$-\upsilon\varepsilon_{ijk}\gamma_j^l\left(\frac{\partial (\nabla\wedge\mathbf{q})_k}{\partial \xi^l} - (\nabla\wedge\mathbf{q})_m\, E_{mkl}\right) \qquad (2)$$

where the physical components of $\nabla\wedge\mathbf{q}$ are defined by

$$(\nabla\wedge\ \mathbf{q})_i = \varepsilon_{ijk}\ \gamma_j^l\ \left(\frac{\partial q_k}{\partial \xi^l} - q_m E_{mkl}\right) \qquad (3)$$

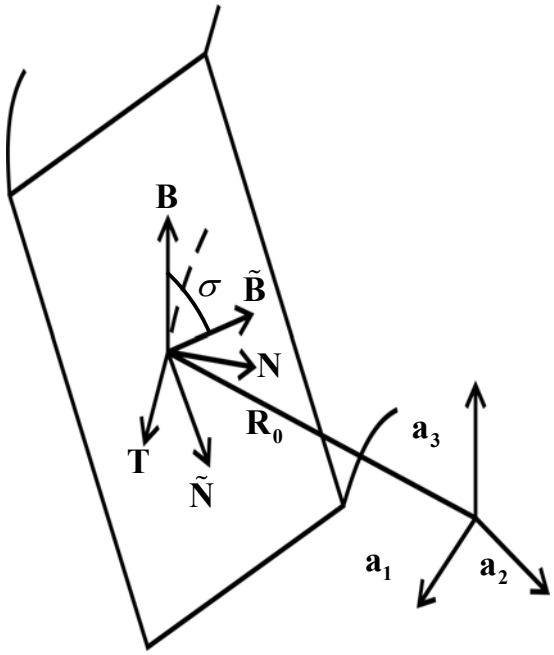

Fig 2. Various vectors related to the centre line of a duct.

Let the centre line of the duct be the smooth space curve $\mathbf{R}_0(s)$, where the parameter $'s'$ is the arc-length. The unit tangent $\mathbf{T}$, normal $\mathbf{N}$ and binormal $\mathbf{B}$ vectors of the space curve $\mathbf{R}_0(s)$ are given by the relations

$$\mathbf{T}(s) = \frac{d\mathbf{R}_0}{ds},\ \mathbf{N}(s) = \frac{1}{\kappa}\frac{d\mathbf{T}}{ds},\ \mathbf{B}(s) = \mathbf{T}\wedge\mathbf{N} \quad (4)$$

The curvature κ and torsion τ are determined by the Serret-Frenet formulae

$$\frac{d\mathbf{T}}{ds} = \kappa\mathbf{N},\ \frac{d\mathbf{N}}{ds} = \tau\mathbf{B} - \kappa\mathbf{T},\ \frac{d\mathbf{B}}{ds} = -\tau\mathbf{N} \qquad (5)$$

Let x be a coordinate along the direction of $\tilde{\mathbf{N}}$ and y be a coordinate along the direction of $\tilde{\mathbf{B}}$. Here $\tilde{\mathbf{N}}$ and $\tilde{\mathbf{B}}$ are the orthogonal unit vectors obtained by a rotation of the physical basis vector $\mathbf{N}$ and $\mathbf{B}$ with the angle $\sigma(s)$ in the $\mathbf{N}-\mathbf{B}$ plane which is shown in Fig 2. Therefore, we have

$$\left.\begin{aligned}\tilde{\mathbf{N}} &= \cos\sigma\,\mathbf{N} - \sin\sigma\,\mathbf{B}\\ \tilde{\mathbf{B}} &= \sin\sigma\ \mathbf{N} + \cos\sigma\ \mathbf{B}\end{aligned}\right\} \qquad (6)$$

The position vector $\mathbf{R}$ of any points in the duct is thus written in the following form:

$$\mathbf{R}(s,x,y) = \mathbf{R}_0(s) + x\tilde{\mathbf{N}}(s) + y\tilde{\mathbf{B}}(s) \qquad (7)$$

The variables are non-dimensionalised by the characteristic length a (half width) and the kinematic viscosity υ as follows:

$$\left.\begin{array}{l} u=\dfrac{\upsilon}{a}u',\ v=\dfrac{\upsilon}{a}v',\ w=\dfrac{\upsilon}{a}\dfrac{w'}{\sqrt{2\kappa'}} \\ \kappa=\dfrac{\kappa'}{a},\ \tau=\dfrac{\tau'}{a},\ p=\rho\dfrac{\upsilon^2}{a^2}p' \\ s=s'a,\quad x=x'a,\quad y=y'a \end{array}\right\} \tag{8}$$

Here w',u',v' are non-dimensional velocity components in the direction of s',x',y' respectively and p',κ',τ' are the non-dimensional pressure, curvature and torsion respectively. The variables without prime are the dimensional quantities. For the incompressible fully developed flow, the velocity is independent of s'.We further introduce a new variable $y'=\gamma\,\overline{y}$, where $\gamma\left(=\dfrac{b}{a}\right)$ is the aspect ratio of the cross-section. Since the flow field is uniform in the axial direction, we can introduce a stream function $\psi=\psi(x',y')$ such that

$$\left.\begin{array}{l} \dfrac{\partial\psi}{\partial y'}=Ju'\sqrt{2\kappa'}+\tau' y' w' \\ -\dfrac{\partial\psi}{\partial x'}=Jv'\sqrt{2\kappa'}-\tau' x' w' \end{array}\right\} \tag{9}$$

where $J=1-\kappa' x'$.

Therefore, the basic equations for w' and ψ are derived from the Navier-Stokes equations as follows:

$$\begin{aligned}
&D_n-\frac{\tau' x'}{J}\left(1+\frac{\tau'^2\gamma^2\overline{y}^2}{J^2}\right)\psi_{x'x'x'}-\frac{\tau'\overline{y}}{J}\left(1+\frac{\tau'^2\gamma^2\,\overline{y}^2}{J^2}-\frac{2\tau'^2x'^2}{J^2}\right)\psi_{x'x'\overline{y}}\\
&-\frac{\tau'\overline{y}}{J\gamma^2}\left(\frac{\tau'^2x'^2}{J^2}+1\right)\psi_{\overline{y}\overline{y}\overline{y}}+\frac{\tau' x'}{J\gamma^2}\left(\frac{2\tau'^2\gamma^2\,\overline{y}^2}{J^2}-1-\frac{\tau'^2x'^2}{J^2}\right)\psi_{x'\overline{y}\overline{y}}\\
&-\frac{3\kappa'\tau'\overline{y}}{J^2}\left(1+\frac{\tau'^2\gamma^2\overline{y}^2}{J^2}-\frac{2\tau'^2x'}{\kappa' J}-\frac{\tau'^2x'^2}{J^2}\right)\psi_{x'\overline{y}}\\
&-\frac{\tau'}{J^2}\left(\frac{2\tau'^2\gamma^2\overline{y}^2}{J}+\kappa' x'+\frac{3\kappa'\tau'^2x'\gamma^2\,\overline{y}^2}{J^2}-\frac{\tau'^2x'^2}{J}\right)\psi_{x'x'}\\
&+\frac{\tau'}{J\gamma^2}\left(\frac{3\kappa'\tau'^2x'\gamma^2\overline{y}^2}{J^3}-\frac{2\tau'^2x'^2}{J^2}+2\kappa' x'+\frac{\tau'^2\gamma^2\,\overline{y}^2}{J^2}\right)\psi_{\overline{y}\overline{y}}\\
&-\frac{\tau'\overline{y}}{J^3}\left(\frac{3\kappa'^2\tau'^2\gamma^2\,\overline{y}^2}{J^2}-\frac{4\kappa'\tau'^2x'}{J}-\tau'^2+3\kappa'^2\right)\psi_{\overline{y}}\\
&-\frac{\tau'}{J^2}\left(\frac{3\kappa'\tau'^2\gamma^2\overline{y}^2}{J^2}+\frac{\kappa'^2x'}{J}+\frac{3\kappa'^2\tau'^2x'\gamma^2\overline{y}^2}{J^3}-\frac{\kappa'\tau'^2x'^2}{J^2}\right.\\
&\left.-\frac{\tau'^2x'}{J}+\kappa'\right)\psi_{x'}-\frac{2\tau'^2x'\,\overline{y}}{J}\left(\frac{\tau'^2\gamma^2\overline{y}^2}{J^2}+\frac{\tau'^2x'^2}{J^2}+1\right)w'_{x'\overline{y}}\\
&+\left(\frac{2\tau'^2\gamma^2\overline{y}^2}{J}+\frac{\tau'^4\gamma^4\overline{y}^4}{J^3}+\frac{\tau'^2x'^2}{J}+\frac{\tau'^4x'^2\gamma^2\overline{y}^2}{J^3}+J\right)w'_{x'x'}\\
&+\left(\frac{\tau'^2\overline{y}^2}{J}+\frac{\tau'^4x'^2\overline{y}^2}{J^3}+\frac{2\tau'^2x'^2}{J\gamma^2}+\frac{J}{\gamma^2}+\frac{\tau'^4x'^4}{J^2\gamma^2}\right)w'_{\overline{y}\overline{y}}\\
&+\left(\frac{3\kappa'\tau'^4\gamma^4\overline{y}^4}{J^4}+\frac{\tau'^2x'}{J}-\frac{\tau'^4x'\gamma^2\overline{y}^2}{J^3}+\frac{2\kappa'\tau'^2\gamma^2\overline{y}^2}{J^2}+\frac{\kappa'\tau'^2x'^2}{J^2}\right.\\
&\left.+\frac{3\kappa'\tau'^4x'^2\gamma^2\overline{y}^2}{J^4}-\kappa'-\frac{\tau'^4x'^4}{J^3}\right)w'_{x'}+\frac{\tau'^2}{J}\left(-\frac{\kappa'x'\overline{y}}{J}-\frac{\tau'^2x'^2\overline{y}}{J^2}+\overline{y}\right.\\
&\left.-\frac{\tau'^2\gamma^2\,\overline{y}^3}{J^2}-\frac{3\kappa'\tau'^2x'\gamma^2\,\overline{y}^3}{J^3}-\frac{3\kappa'\tau'^2x'^2\overline{y}}{J^3}\right)w'_{\overline{y}}+\frac{\kappa'}{J}\left(\frac{3\kappa'\tau'^4\gamma^4\,\overline{y}^4}{J^4}\right.\\
&\left.-\frac{\tau'^4x'\gamma^2\,\overline{y}^2}{J^3}-\frac{\kappa'\tau'^2\gamma^2\overline{y}^2}{J^2}+\frac{\tau'^2x'}{J}+\frac{\kappa'\tau'^2x'^2}{J^2}-\kappa'\right.\\
&\left.+\frac{3\kappa'\tau'^4x'^2\gamma^2\,\overline{y}^2}{J^4}-\frac{\tau'^4x'^3}{J^3}+\frac{3\kappa'\tau'^2\gamma^2\,\overline{y}^2}{J^2}\right)w'\\
&-\frac{1}{\gamma\sqrt{2\kappa'}}\left[\left(\frac{\tau'^2x'^2}{J^2}+\frac{\tau'^2\gamma^2\,\overline{y}^2}{J^2}+1\right)w'_{x'}\psi_{\overline{y}}\right.\\
&-\frac{\kappa'\tau'x'}{J^3}\psi_{x'}\psi_{\overline{y}}\left(\frac{\kappa'\tau'^2x'^2}{J^3}+\frac{\kappa'\tau'^2\gamma^2\,\overline{y}^2}{J^3}-\frac{\kappa'}{J}+\frac{2\tau'^2x'}{J^2}\right)w'\psi_{\overline{y}}\\
&\left.-\left(\frac{\tau'^2x'^2}{J^2}+\frac{\tau'^2\gamma^2\,\overline{y}^2}{J^2}+1\right)w'_{\overline{y}}\psi_{x'}\right]-\frac{\tau'}{J^2\sqrt{2\kappa'}}\left(\frac{\overline{y}}{\gamma}\psi_{x'}\psi_{\overline{y}\overline{y}}\right.\\
&+\frac{x'}{\gamma}\psi_{x'}\psi_{x'\overline{y}}-\frac{\overline{y}}{\gamma}\psi_{\overline{y}}\psi_{x'\overline{y}}-2\tau'\gamma\,\overline{y}\,w'\psi_{x'}-\frac{x'}{\gamma}\psi_{\overline{y}}\psi_{x'x'}\Big)\\
&+\frac{\kappa'\tau'\overline{y}}{J^3\gamma\sqrt{2\kappa'}}\psi_{\overline{y}}^2=0
\end{aligned}\tag{10}$$

$$\begin{aligned}
&\frac{1}{J\sqrt{2\kappa'}}\left[\left(1+\frac{\tau'^2\gamma^2\overline{y}^2}{J^2}\right)\psi_{x'x'x'x'}+\left(1+\frac{\tau'^2x'^2}{J^2}\right)\frac{1}{\gamma^4}\psi_{\overline{y}\overline{y}\overline{y}\overline{y}}\right]\\
&-\frac{2\tau'^2x'\,\overline{y}}{J^3\sqrt{2\kappa'}}\psi_{x'x'x'\overline{y}}+\frac{1}{J\sqrt{2\kappa'}}\left(\frac{\tau'^2x'^2}{J^2}+2+\frac{\tau'^2\gamma^2\,\overline{y}^2}{J^2}\right)\frac{1}{\gamma^2}\psi_{x'x'\overline{y}\overline{y}}\\
&-\frac{2\tau'^2\,x'\,\overline{y}}{J^3\gamma^2\sqrt{2\kappa'}}\psi_{x'\overline{y}\overline{y}\overline{y}}+\frac{1}{J^2\sqrt{2\kappa'}}\left(2\kappa'+\frac{6\kappa'\tau'^2\gamma^2\overline{y}^2}{J^2}\right.\\
&\left.-\frac{\tau'^2x'}{J}\right)\psi_{x'x'x'}+\frac{1}{J^2\sqrt{2\kappa'}}\left(\frac{3\kappa'\tau'^2x'^2}{J^2}+\frac{3\kappa'\tau'^2\gamma^2\,\overline{y}^2}{J^2}+2\kappa'\right.\\
&\left.-\frac{\tau'^2x'}{J}\right)\frac{1}{\gamma^2}\psi_{x'\overline{y}\overline{y}}-\frac{\tau'^2\,\overline{y}}{J^3\sqrt{2\kappa'}}\left(\frac{9\kappa'x'}{J}+1\right)\psi_{x'x'\overline{y}}\\
&-\frac{\tau'^2\overline{y}}{J^3\gamma^2\sqrt{2\kappa'}}\left(\frac{3\kappa'x'}{J}+1\right)\psi_{\overline{y}\overline{y}\overline{y}}+\frac{\kappa'}{J^3\sqrt{2\kappa'}}\left(3\kappa'+\frac{15\kappa'\tau'^2\gamma^2\overline{y}^2}{J^2}\right.\\
&\left.-\frac{4\tau'^2x'}{J}\right)\psi_{x'x'}+\frac{\kappa'\tau'^2}{J^4\gamma^2\sqrt{2\kappa'}}\left(2x'+\frac{3\kappa'\gamma^2\,\overline{y}^2}{J}\right)\psi_{\overline{y}\overline{y}}\\
&-\frac{6\kappa'\tau'^2\overline{y}}{J^4\sqrt{2\kappa'}}\left(\frac{2\kappa'x'}{J}+1\right)\psi_{x'\overline{y}}+\frac{\kappa'}{J^4\sqrt{2\kappa'}}\left(-\frac{4\kappa'\tau'^2x'}{J}+3\kappa'^2\right.\\
&\left.+\frac{15\kappa'^2\tau'^2\gamma^2\,\overline{y}^2}{J^2}-\tau'^2\right)\psi_{x'}-\frac{\kappa'\tau'}{J^3\sqrt{2\kappa'}}\left(4\kappa'+\frac{3\kappa'^2x'}{J}\right.\\
&+\frac{15\kappa'^2\tau'^2x'\gamma^2\,\overline{y}^2}{J^3}-\frac{4\kappa'\tau'^2x'^2}{J^2}+\frac{12\kappa'\tau'^2\gamma^2\overline{y}^2}{J^2}\\
&\left.-\frac{3\tau'^2x'}{J}\right)w'-\frac{6\kappa'^2\tau'^2\overline{y}}{J^5\sqrt{2\kappa'}}\psi_{\overline{y}}-\frac{\tau'}{J^2\sqrt{2\kappa'}}\left(4\kappa'+\frac{15\kappa'^2\tau'^2x'\gamma^2\,\overline{y}^2}{J^3}\right.
\end{aligned}$$

$$+\frac{3\kappa'^2x'}{J}-\frac{4\kappa'\tau'^2x'^2}{J^2}-\frac{3\tau'^2x'}{J}+\frac{12\tau'^2\kappa'\gamma^2\bar{y}^2}{J^2}\Bigg)w'_{x'}$$
$$+\frac{\tau'\bar{y}}{J^3\sqrt{2\kappa'}}\Bigg(\frac{12\kappa'^2\tau'^2x'^2}{J^2}+\frac{16\kappa'\tau'^2x'}{J}+3\tau'^2$$
$$+\kappa'^2-\frac{3\kappa'^2\tau'^2\gamma^2\bar{y}^2}{J^2}\Bigg)w'_{\bar{y}}+\frac{\tau'\bar{y}}{J^2\sqrt{2\kappa'}}\Bigg(\frac{9\kappa'\tau'^2x'^2}{J^2}+\frac{10\tau'^2x'}{J}$$
$$-\frac{3\kappa'\tau'^2\gamma^2\bar{y}^2}{J^2}+\kappa'\Bigg)w'_{x'\bar{y}}-\frac{\tau'}{J^2\sqrt{2\kappa'}}\Bigg(\frac{6\kappa'\tau'^2x'\gamma^2\bar{y}^2}{J^2}+2\kappa'x'$$
$$+4J+\frac{4\tau'^2\gamma^2\bar{y}^2}{J}-\frac{\tau'^2x'^2}{J}\Bigg)w'_{x'x'}-\frac{\tau'}{J\sqrt{2\kappa'}}\Bigg(\frac{4}{\gamma^2}+\frac{3\kappa'x'}{J\gamma^2}+\frac{4\tau'^2x'^2}{\gamma^2J^2}$$
$$+\frac{3\kappa'\tau'^2x'^2}{\gamma^2J^3}-\frac{\tau'^2\bar{y}^2}{J^2}-\frac{3\tau'^2\kappa'x'\bar{y}^2}{J^3}\Bigg)w'_{\bar{y}\bar{y}}+\frac{\tau'x'}{J\sqrt{2\kappa'}}\Bigg(\frac{2\tau'^2\bar{y}^2}{J^2}$$
$$-\frac{\tau'^2x'^2}{\gamma^2J^2}-\frac{1}{\gamma^2}\Bigg)w'_{x'\bar{y}\bar{y}}-\frac{\tau'x'}{J\sqrt{2\kappa'}}\Bigg(1+\frac{\tau'^2\gamma^2\bar{y}^2}{J^2}\Bigg)w'_{x'x'x'}$$
$$+\frac{\tau'\bar{y}}{J\sqrt{2\kappa'}}\Bigg(\frac{2\tau'^2x'^2}{J^2}-1-\frac{\tau'^2\gamma^2\bar{y}^2}{J^2}\Bigg)w'_{x'x'\bar{y}}$$
$$-\frac{\tau'\bar{y}}{J\gamma^2\sqrt{2\kappa'}}\Bigg(1+\frac{\tau'^2x'^2}{J^2}\Bigg)w'-\frac{1}{\gamma^3J^3}\psi_{\bar{y}}\psi_{\bar{y}\bar{y}\bar{y}}-\frac{3}{2\gamma J^3}\psi_{\bar{y}}\psi_{x'x'_{\bar{y}\bar{y}\bar{y}}}$$
$$+\frac{\tau'}{\gamma J^2}\Bigg(\frac{2}{\kappa'}+\frac{3x'}{2J}\Bigg)w_{x'}\psi_{\bar{y}}-\frac{3\kappa'}{2\gamma J^4}\psi_{x'}\psi_{\bar{y}}-\frac{1}{2\kappa'\gamma^3J^2}\psi_{x'_{\bar{y}\bar{y}}}\psi_{\bar{y}}$$
$$+\frac{1}{2\kappa'\gamma^3J^2}\psi_{x'}\psi_{\bar{y}\bar{y}\bar{y}}-\frac{1}{2\kappa'\gamma J^2}\psi_{\bar{y}}\psi_{x'x'x'}+\frac{1}{2\gamma J^3}\psi_{x'}\psi_{x'\bar{y}}$$
$$-\frac{\tau'}{\gamma J^2}\Bigg(\frac{2}{\kappa'}+\frac{x'}{J}\Bigg)w'_{\bar{y}}\psi_{x'}+\frac{1}{2\kappa'\gamma J^2}\psi_{x'}\psi_{x'x'\bar{y}}+\frac{\tau'\bar{y}}{2\kappa'\gamma J^2}w'_{x'\bar{y}}\psi_{\bar{y}}$$
$$+\frac{\tau'x'}{2\gamma J^3}w'\psi_{x'\bar{y}}+\frac{3\tau'}{\gamma J^3}\Bigg(1+\frac{\kappa'x'}{2J}\Bigg)w'\psi_{\bar{y}}+\frac{\tau'x'}{2\kappa'\gamma J^2}w'_{x'}\psi_{x'\bar{y}}$$
$$-\frac{\tau'\bar{y}}{2\kappa'\gamma J^2}w'_{\bar{y}}\psi_{x'\bar{y}}-\frac{1}{\gamma J}\Bigg(1-\frac{\tau'^2x'}{\kappa'J}\Bigg)w'w'_{\bar{y}}-\frac{\tau'^2\gamma\bar{y}}{J^3}w'^2$$
$$-\frac{\tau'^2\gamma\bar{y}}{\kappa'J^2}w'w'_{x'}+\frac{\tau'\bar{y}}{2\gamma J^3}w'\psi_{\bar{y}\bar{y}}+\frac{\tau'\bar{y}}{2\kappa'\gamma J^2}w'_{x'}\psi_{\bar{y}\bar{y}}+\frac{\tau'\bar{y}}{2\gamma J^3}w'_{\bar{y}}\psi_{\bar{y}}$$
$$-\frac{\tau'\bar{y}}{2\kappa'\gamma J^2}w'_{\bar{y}\bar{y}}\psi_{x'}+\frac{\tau'x'}{2\kappa'\gamma J^2}w'_{x'x'}\psi_{\bar{y}}-\frac{\tau'x'}{2\kappa'\gamma J^2}w'_{x'\bar{y}}\psi_{x'}=0 \tag{11}$$

3. METHOD OF NUMERICAL CALCULATIONS

The spectral method is applied in the present numerical calculation. The expansion by polynomial functions is utilized to obtain steady solution. Variables are expanded in series of functions consisting of Chebyshev polynomials. We expand $w(x',\bar{y})$ and $\Psi(x',\bar{y})$ as

$$\left.\begin{aligned} w'(x',\bar{y}) &= \sum_{m=0}^{M}\sum_{n=0}^{N} w_{mn}\,\Phi_m(x')\,\Phi_n(\bar{y}) \\ \Psi(x',\bar{y}) &= \sum_{m=0}^{M}\sum_{n=0}^{N} \psi_{mn}\,\Psi_m(x')\,\Psi_n(\bar{y}) \end{aligned}\right\} \tag{12}$$

where M and N are the truncation numbers along x' and $\bar{y}$ direction respectively and w_{mn} and ψ_{mn} are the coefficients of expansion.

The expansion functions $\Phi_n(x')$ and $\Psi_n(x')$ are expressed as

$$\Phi_n(x')=(1-x'^2)C_n(x'),\quad \Psi_n(x')=(1-x'^2)^2C_n(x') \tag{13}$$

where $C_n(x')=\cos(n\cos^{-1}(x'))$ is the n-th order Chebyshev polynomial.

In order to obtain the solutions for w_{mn} and ψ_{mn}, the expansion series (12) are then substituted into the basic equations (10) and (11) and apply the collocation method (Gottlieb and Orszag[11]), then we obtain the non-linear algebraic equations for w_{mn} and ψ_{mn} .The collocation points are taken as:

$$\left.\begin{aligned} x'_i &= \cos\frac{\pi i}{M+2}, \qquad (i=1,\cdots\cdots,M+1) \\ \bar{y}_j &= \cos\frac{\pi j}{M+2}, \qquad (j=1,\cdots\cdots\cdots,N+1) \end{aligned}\right\}$$

The non-linear algebraic equations for w_{mn} and ψ_{mn} are solved by the Newton-Raphson method starting with an initial guess of the solution.

The convergence is assured by taking $\in_{\bar{p}}<10^{-8}$, where subscript $\bar{p}$ denotes the iteration number and $\in_{\bar{p}}$ is defined as

$$\in_{\bar{p}}=\sum_{m=0}^{M}\sum_{n=0}^{N}\left[\left(w_{mn}^{(\bar{p}+1)}-w_{mn}^{(\bar{p})}\right)^2+\left(\Psi_{mn}^{(\bar{p}+1)}-\Psi_{mn}^{(\bar{p})}\right)^2\right] \tag{14}$$

4. FLUX THROUGH THE HELICAL DUCT

The dimensional total flux, Q' through the duct is obtained as:

$$Q'=\int_{-a\gamma}^{a\gamma}\int_{-a}^{a}w'dxdy \tag{15}$$

where, w' is the component of the velocity normal to $x'-y'$ plane and the dimensionless total flux is

$$Q=\gamma\int_{-1}^{1}\int_{-1}^{1}w'(x',\bar{y})\,dx'd\,\bar{y} \tag{16}$$

The non-dimensional Resistance coefficient (R_c) takes the following form

$$R_c=\frac{128\gamma\sqrt{2k}}{1+\gamma}D_n\frac{1}{\left(\int_{-1}^{1}\int_{-1}^{1}w(x',\bar{y})\,dx'd\bar{y}\right)^2} \tag{17}$$

5. RESULTS AND DISCUSSION

Left-handed helical duct with rectangular cross-section has been taken to investigate the flow characteristics for wide range of Dean number (D_n), fixed curvature $(\kappa'=0.1)$, different torsions $(\tau'=0.0,0.1)$ and aspect ratio $(\gamma=1.5)$. In this article, the left side is the outer wall and the right side is the inner wall of the cross-section of the duct.

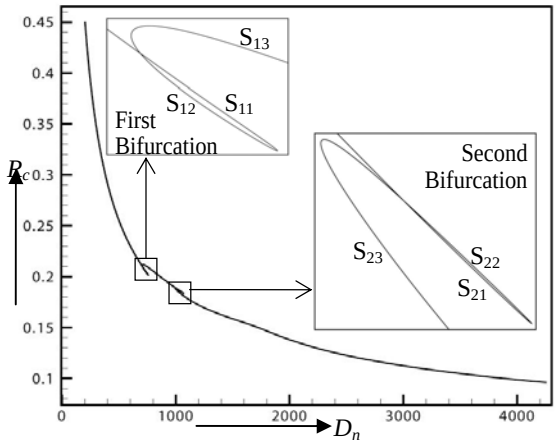

Fig 3. Solution Curve for steady fluid flow in Curved duct for $\kappa' = 0.1, \gamma = 1.5, \tau' = 0.1$ and $0 \le D_n \le 4258$.

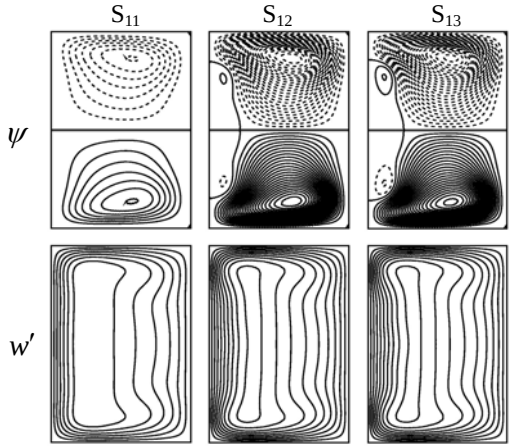

Fig 4. Stream lines of the secondary flow and contour plots of the axial flow on solution curves at $D_n = 706$.

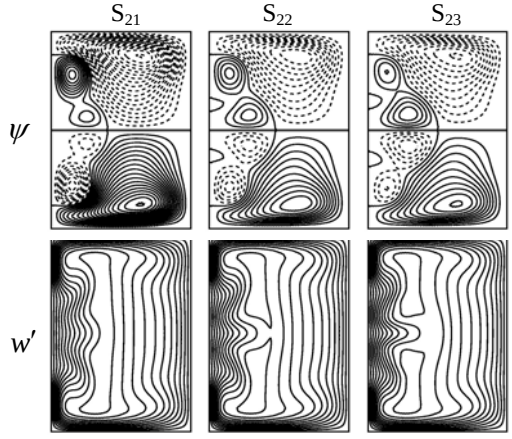

Fig 5. Stream lines of the secondary flow and contour plots of the axial flow on solution curves at $D_n = 1005$.

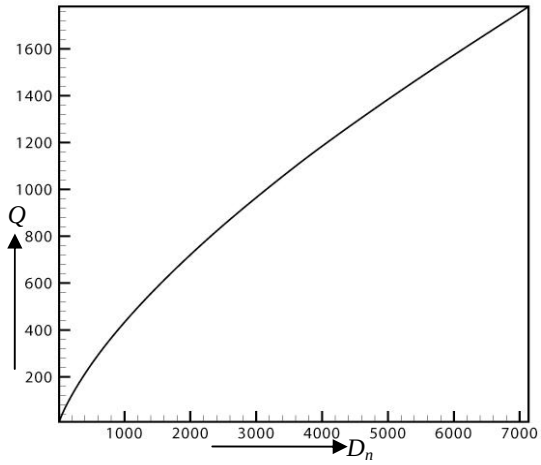

Fig 6. Solution Curve of steady flow through a helical rectangular duct for $\kappa' = 0.1$, $\gamma = 1.50$ $\tau' = 0.1$ and $0 \le D_n \le 7134$.

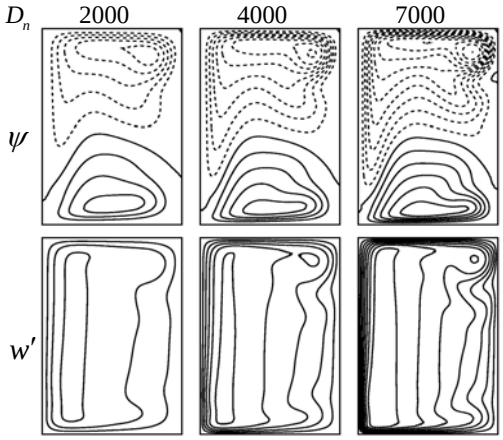

Fig 7. Stream lines of the secondary flow and contour plots of the axial flow on the solution curve for $\gamma = 1.5$, $\kappa' = 0.1$ and $\tau' = 0.1$ for various Dean number.

5.1 Case I $(\kappa' = 0.1,\ \tau' = 0.0$ **and** $\gamma = 1.5)$

Fig. 3 shows that the resistance coefficient (R_c) through the duct versus Dean number (D_n) and this is called solution curve. In this solution curve two bifurcation areas have been obtained which are the most important characteristic of the flow in the duct. After a comprehensive study over a parametric space, steady solution curve is obtained for $\kappa' = 0.1, \tau' = 0.0, \gamma = 1.5$ and Dean number in the range of $0 \le D_n \le 4258$. In order to visualize the bifurcation areas more explicitly the enlargement of the solution curve areas are necessary. The above mentioned numerical solution curve areas are obtained by arc-length method as discussed in Keller et. al [12]. In fig. 3 it is seen that resistance coefficient decreases as Dean number increases along the curves S_{11}, S_{13}, S_{21} & S_{23} and resistance coefficient increases as

Dean number decreases along the curves S_{12}, S_{22} in the bifurcation areas. From fig. 4 it is seen that the secondary flow patterns consists of two-vortex, four-vortex with two minor very weak vortices and four-vortex with two minor weak vortices for same Dean number $D_n = 706$. It is clear that weak vortices have been created near the outer wall of the cross-section and axial flow is gradually shifted towards the outer wall of the cross-section. In fig.5 It is seen that four-vortex secondary flow patterns are found along the curve S_{21} while six-vortex secondary flow patterns are observed along the curves S_{22} and S_{23} for same Dean number $D_n = 1005$. The axial flow is shifted more quickly to the outer wall of the cross-section. It is also seen that axial flow is stronger near the outer wall on the curves S_{22} and S_{23}.

5.2 Case II $(\kappa' = 0.1,\ \tau' = 0.1$ and $\gamma = 1.5)$

The solution curve (Dean number versus flux) is depicted in the fig. 6. In this figure it is seen that steady solutions are found in the range of $0 \le D_n \le 7134$. It is also observed that the flux increases as Dean number increases. The secondary and axial flow patterns on the solution curve are shown in fig. 7. In these flow patterns ψ and w' are drawn with $\Delta\psi = 1.75$ and $\Delta w' = 90.0$. Two-vortex non-symmetric secondary flow patterns are found on the solution curve for several Dean numbers and maximum axial flow is shifted to the lower part of the outer wall of the cross-section.

6. CONCLUSIONS

According to the present results, we can draw the following Concluding remarks:

- Several pair of vortices has been found in the bifurcation areas due to centrifugal and pressure gradient forces.
- Axial flow is shifted quickly to the outer wall of the cross-section for large Dean number.
- Torsion causes the distortion of the symmetry of the flow enlarging the upper vortex to the expenses of the lower vortex.
- The multiple solutions have not been found for torsion 0.1 and aspect ratio 1.5.

7. REFERENCES

1. Dean, W. R., 1927, "Note on the motion of fluid in a curved pipe", Philosophical magazine and Journal of Science, 4(20): 208-223.
2. Berger, S. A., Talbot, L. and Yao, L. S., 1983, "Flow in curved pipes", Annual Reviews of fluid Mechanics, 15**:** 461-512.
3. Ito, H., 1987, "Flow in curved pipes", JSME International Journal, 30(262): 543-552.
4. Cheng, K. C., Lin, R. and Ou, J. W., 1975, "Graetz problem in curved square channels", Trans. ASME Journal of heat transfer, 97: 244-248.
5. Yang, T. and Wang, L., 2001, "Solution Structure and Stability of Viscous Flow in Curved Square Ducts", ASME Journal of Fluids Engineering, 123: 863-868.
6. Wang, C. Y., 1981, "On the low-Reynolds number flow in a helical pipe", Journal of Fluid Mechanics, 108:185-194.
7. Bolinder, C. J. and Sunden, B., 1995, "Flow visualization and LDV measurements of laminar flow in a helical square duct with finite pitch", Experimental Thermal and Fluid Science, 11: 348-363.
8. Sakalis, V. D., Hatzikonstantinou, P. M. and Papadopoulos, P. K., 2005, "Numerical Procedure for the Laminar Developed Flow in a Helical Square Duct", Journal of Fluids Engineering, 127: 136-148.
9. Bhattacharjee, P. K. and Alam, M. M., 2008, "Torsion Effect on Fluid Flow in a Helical Pipe with Square Cross-section", *Proc. 4th BSME-ASME Int. Comf. on Thermal Engineering*, pp. I: 198-203.
10. Wang, J. W. and Andrews, J. R. G., 1995, "Numerical Simulation of Flow in Helical Ducts", AIChE Journal, 41(5): 1071-1080.
11. Gottlieb, D. and Orszag, S. A., 1977, "Numerical Analysis of Spectral Methods", *Society for Industrial and Applied Mathematics*, Philadelphia.
12. Keller, H. B., 1987, "Lectures on Numerical Methods in Bifurcation problems", Springer, Berlin.

8. NOMENCLATURE

Symbol	Meaning
D_n	Dean number
γ	Aspect ratio
κ'	Dimensionless curvature
τ'	Dimensionless torsion
w', u', v'	Dimensionless velocity along axial, radial, circumferential direction respectively
s', x', y'	Dimensionless length coordinates along axial, radial, circumferential direction respectively
ψ	Stream function
R_c	Resistance coefficient
Q	Dimensionless total flux

9. MAILING ADDRESS

M. Mahmud Alam
Mathematics Discipline,
Khulna University,
Khulna-9208, Bangladesh
E-mail: alam_mahmud2000@yahoo.com